MODELING FRACTIONAL CRYSTALLIZATION OF BASALTS ALONG THE NORTHERN EAST PACIFIC RISE

Undergraduate Research Thesis
Submitted in partial fulfillment of the requirements for graduation
with research distinction in Earth Sciences
in the undergraduate colleges of
The Ohio State University

By

Harrison F. Love
The Ohio State University
2017

Approved by

Michael Barton, Advisor

School of Earth Sciences

TABLE OF CONTENTS

Abstract……....iii

Acknowledgements……..iv

List of Figures…….……..v

Introduction……..….1

Geologic Setting……..……...….1

Geology…….……..……...…….2

Methods

Sampling Methodology…….4

Location 1 8.3°N-8.8°N……4

Location 2 8.8°N-9.4°N……5

Location 3 9.4°N-10°N…….6

Location 4 10°N-10.6°N……...7

Results

Location 1 8.3°N-8.8°N……8

Location 2 8.8°N-9.4°N……10

Location 3 9.4°N-10°N…….12

Location 4 10°N-10.6°N……...14

Discussion

Effect of Varying MgO in Parental Magma, Location 1…….....15

Effect of Fe-Ti Oxides and Oxygen Fugacity, Location 2….....16

Effect of Adding H_2O to the Parent Magma, Location 3…….16

Modeling Done at Location 4……...18

Conclusions……19

Recommendations for Future Work…….....20

References Cited…..…….…….21

Appendix A……...23

Appendix B……...25

Appendix C……...27

Appendix D……...29

ABSTRACT

Mid-ocean ridges are the locations for formation of the Earth's oceanic crust. The goal of this research is to understand the large and small scale process that occur within and around these ridges. More specifically, this research was conducted to understand the geochemical processes which cause variations in the compositions of oceanic crust from samples collected from the sea floor. This project focuses on the northern part of the East Pacific Rise, or EPR, between 8 and 10 degrees north latitude. In order to better understand the formation of oceanic crust, modeling of the crystallization of liquids which are believed to be close in composition to the most primitive melts erupted in a small area of the ridge has been conducted. The computer program used for modeling is PETROLOG *Danyushevsky and Plechov* (2011). We then compare the composition of the melt as it cools and changes with many thousands of samples collected within the small area of focus. The goal is to find a path of evolution of the simulated liquid which agrees with the compositional trends in our actual samples.

ACKNOWLEDGEMENTS

I would first like to thank my research advisor, Dr. Michael Barton, for taking me on and introducing the process of conducting research. I greatly appreciate all that Dr. Barton and his graduate students; Jameson Scott, Katherine Haines, and Christina Zerda have taught me in the last few years. Dr. Barton has been a great influence for me, and I hope that this research benefits him and his students as much as it has helped me. I would also like to give a special thanks to Scott Hull and Caymen Unterborn of The Ohio State University for providing me with a copy of a python script “AutoMELTS”. Lastly I thank my parents, Martha and Steven Love for encouraging me to think for myself, and helping me achieve my goals, as well as my high school teacher and tennis coach Chris Higgins, who pushed me to be the best person I could be.

LIST OF FIGURES

1. Map of studied region
2. Map of studied region with natural samples overlain
3. Major oxides vs. MgO for high MgO parent, Location 1
4. Major oxides vs. MgO for low MgO parent, Location 1
5. Major oxides vs. MgO with Fe-Ti oxides and fO_2 = -1, Location 2
6. Major oxides vs. MgO with Fe-Ti oxides and fO_2 = +1, Location 2
7. Major oxides vs. MgO with no added H_2O, Location 3
8. Major oxides vs. MgO with added H_2O, Location 3
9. Major oxides vs. MgO, Location 4
10. Modeling major oxides near 9.6°N EPR, *Goss et al. 2010*

A1. K_2O and P_2O_5 vs. MgO for high MgO parent, Location 1
A2. K_2O and P_2O_5 vs. MgO for low MgO parent, Location 1
B1. K_2O and P_2O_5 vs. MgO with Fe-Ti oxides and fO_2 = -1, Location 2
B2. K_2O and P_2O_5 vs. MgO with Fe-Ti oxides and fO_2 = +1, Location 2
C1. K_2O and P_2O_5 vs. MgO with no added H_2O, Location 3
C2. K_2O and P_2O_5 vs. MgO with added H_2O, Location 3
D1. K_2O and P_2O_5 vs. MgO, Location 4

INTRODUCTION

Knowledge of the evolutionary history of magmas is essential for constructing realistic models for the creation and composition of new crust at mid-ocean ridges. Modeling the evolution of magmas at mid-ocean ridges has been done in the past *Herzberg et al.* (2004); *Goss et al.* (2010), but it often appears as a single figure, in papers that were not focused on magma modeling. This study presents a comprehensive overview of petrologic modeling as it applies to mid-ocean ridge basalts. The goal of this study is to model the evolution of mid-ocean ridge magmas and to constrain the pressures at which these magmas partially crystallize en-route to the surface. It has long been known that olivine, plagioclase feldspar, and clinopyroxene are the first minerals to form many basalts *Bowen,* (1956); *Yoder & Tilley,* (1962). Other minerals such as ilmenite and magnetite may crystallize much later in the process, but still can affect the compositions observed in MORB glasses. Variables other than pressure such as the H_2O content of the magma and the oxygen fugacity of the magma will affect mineral stability at a given temperature and pressure, and thus, must also be considered. The results of this study provide information about magma plumbing systems beneath ridges and about the depth of accretion of oceanic crust.

GEOLOGIC SETTING

Geology

The northern East Pacific Rise (nEPR) is classified as a fast spreading ridge *Macdonald,* (2001), with full spreading rates ranging from 9cm/yr to 11cm/yr. The axis of the ridge sits at an average of 2,400 m above the surrounding seafloor. As with other fast spreading ridges, the nEPR does not have an axial valley. Instead there is an axial high, believed to be caused by the increased magma flux at fast spreading rates *Macdonald,* (2001). The magmas formed at mid-ocean ridges are the result of decompression melting in the mantle below the base of the crust. The drop in pressure is the result of crustal thinning near the axis of the ridge, reducing the lithostatic pressure. The reduced pressure coupled with the high temperatures of the upper mantle cause the rock to melt. The width ranges from 200 km to 600 km along the length of the ridge, in the studied region of 8.3°N to 10.6°N this range shows little variation. The height of the ridge decreases at a consistent rate away from the axis due to a density increase that results from crustal cooling. The crust continues to subside until its density equilibrates and forms the abyssal plains of the ocean. This study focused on a region of the nEPR from 8.3°N–10.6°N. The region is bounded by two large transform faults which offset the ridge, the left-stepping Siqueiros to the south, and the right-stepping Clipperton to the north. Between the two transforms, at 9°N, there is an overlapping spreading center.

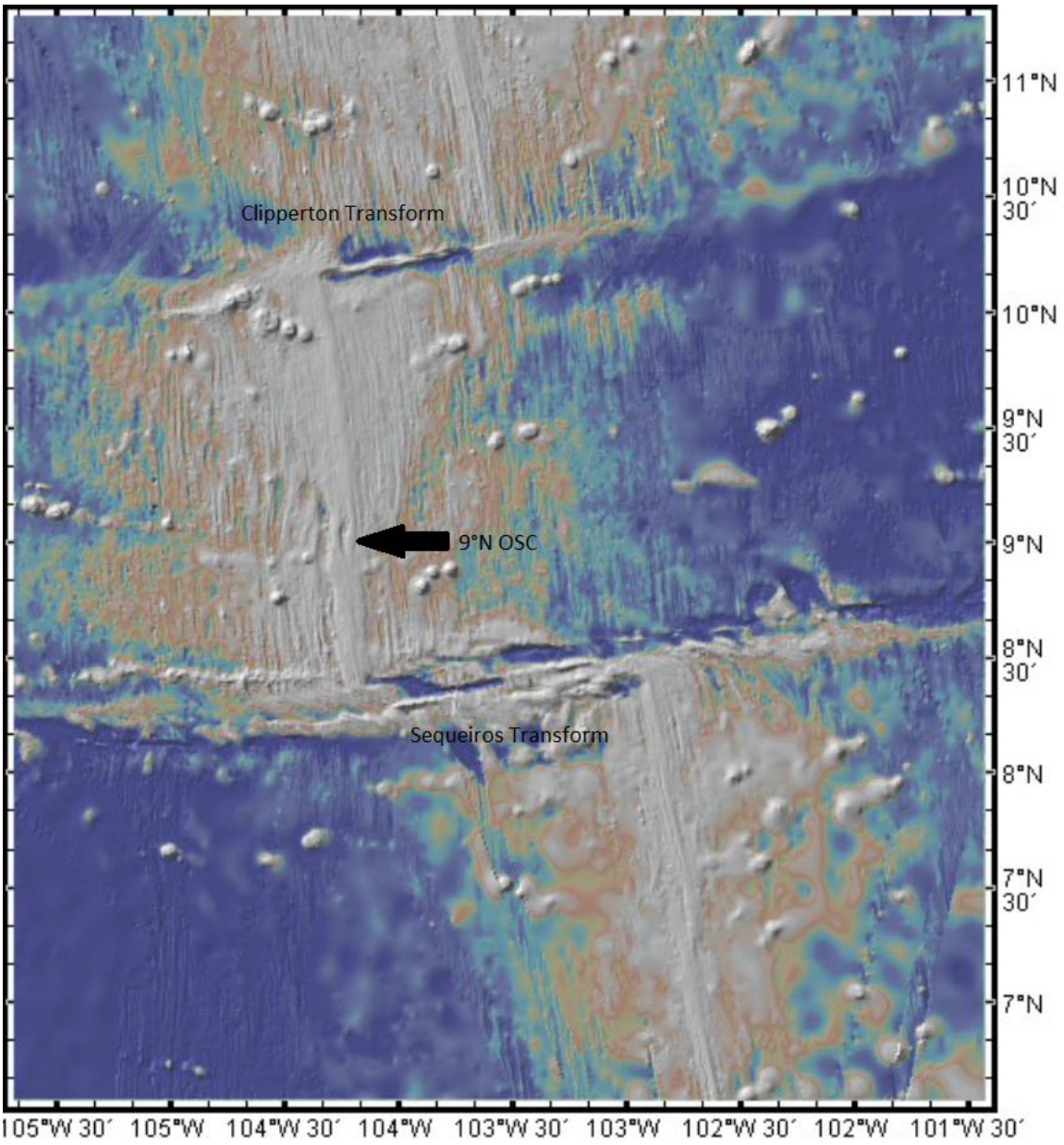

Figure 1. Map showing the region of study on the northern East Pacific Rise, also showing the locations of the two major transforms: the Siqueiros and the Clipperton and the 9°N overlapping spreading center.

METHODS

Modeling of major oxide compositions was performed with the PETROLOG program of *Danyushevsky and Plechov* (2011). A parent magma composition was selected for each locality. The parent composition was normalized to 100 wt. % of major oxides, then entered into PETROLOG, and mineral models for olivine, plagioclase, and clinopyroxene were selected. For one location with a wide range of natural glass compositions, mineral models for ilmenite and magnetite also were selected. Next a pressure of crystallization was chosen, as were values for the oxidation state defined relative to values for the Quartz-Fayalite-Magnetite (QFM) oxygen buffer, and for the water content of the initial. Last, the range of crystallization over which calculations were performed was specified.

Sampling Methodology

The results of modeling were compared with the compositions of natural glasses taken from the petdb (earthchem.org/petdb) database. The main dataset used comprises 3,225 analyses of glasses from 2° N to 15.5° N latitude along the East Pacific Rise. Longitudinally the samples are constrained between -107° W to -100° W. The majority of samples were collected either by dredging of the seafloor or from submersibles and are either from eruptions along the ridge, along fracture zones, or from seamounts. Samples from seamounts were collected over a much broader range of longitude due to seamounts remaining active much further from the ridge axis than fracture zones.

Location 1. 8.3° N – 8.8° N

The first sub-region includes 152 glass analyses after filtering by latitude. The parent composition chosen was WASSIQR-003 *Natland,* (1989). The mineral models used for olivine, plagioclase and clinopyroxene were from *Danyushevsky,* (2001). All three minerals were

assumed to experience 100% fractional crystallization. The model for magma redox state was from *Kress and Carmichael,* (1988) as it was believed to be the best of available options, and the reference oxygen buffer was taken as the QFM buffer, shifted -1 log units. Melt densities were calculated using the model of *Lange and Carmichael,* (1987) and the viscosity model used was from *Giordano and Dingwell.* (2003). Crystallization paths were calculated at various pressures of crystallization (0.5 kb, 2kb, and 3kb) with all other parameters kept constant. A second parent was also chosen for this location to compare the effects of differing parental composition on the model. The 2nd parent was sample ALV2384-001 *Perfit et al.,* (1996). All parameters other than initial composition were the same for the 2nd parent.

Location 2. 8.8° N – 9.4° N

The second sub-region included 173 glass analyses. The parent sample was WASRAI2-030-030 *Niu et al.,* (1997). At this location we chose to evaluate the effects of crystallizing the iron-titanium oxides (Fe-Ti oxides), and the effects of shifting the oxygen buffer of the initial melt. In addition to olivine, plagioclase, and clinopyroxene, a mineral model for ilmenite and magnetite had to be selected in PETROLOG. The models chosen for both ilmenite and magnetite were taken from *Ariskin and Barmina,* (1999). Calculations were done at three pressures (0.5kb, 2kb, and 3kb) for a QFM buffer shifted by -1 log units, and one calculation was done at 2kb for the QFM buffer shifted +1 log units. All other PETROLOG parameters and model choices were the same as for location 1.

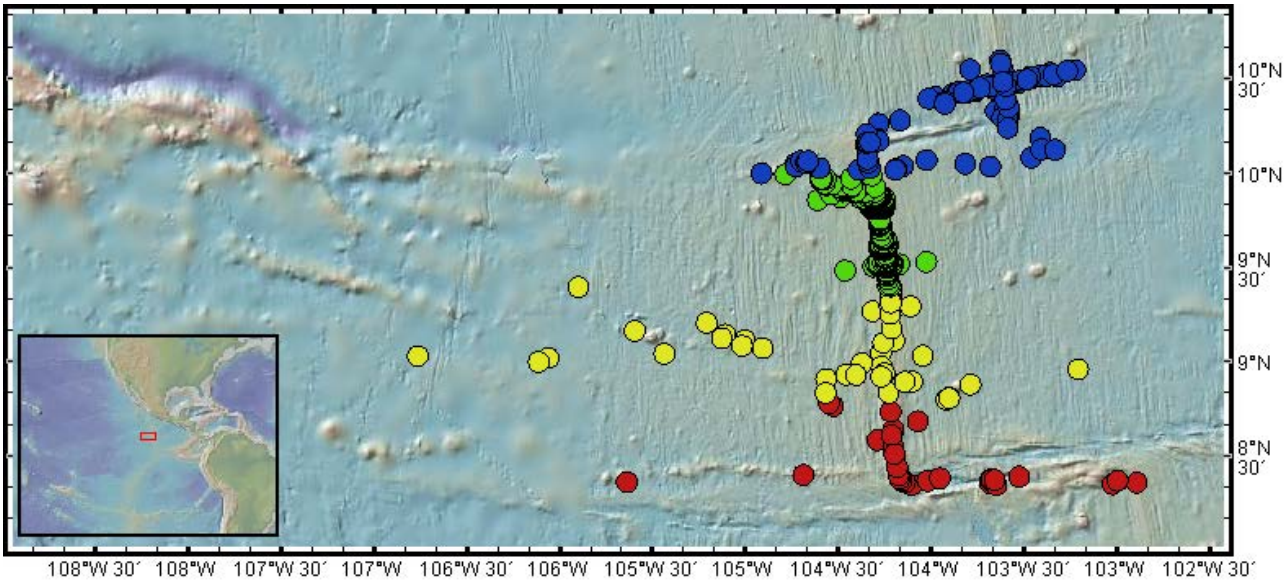

Figure 2. A map showing the area of study on the nEPR with overlain glass analyses for each of the four sub-regions. Red-Location 1, 8.3°N-8.8°N. Yellow-Location 2, 8.8°N-9.4°N. Green-Location 3, 9.4°N-10°N. Blue-Location 4, 10°N-10.6°N.

Location 3. 9.4° N – 10° N

Two different models were calculated for location 3, which is also the most heavily sampled sub-region in the studied area with 829 glass analyses.

Model 1: The first PETROLOG model was the same as used for locations 1 and 2. The parent sample was AII0112-25-003-002 *Allan et al.*, (1989) and all PETROLOG model parameters remained the same as at location 1.

Model 2: The second model used was calculated at 2kb using both PETROLOG and the MELTS software *Ghiorso and Sack,* (1995). The parent for the MELTS model was AII131-11-R455GL *Perfit*, (2000). To compare with the results of the MELTS model, PETROLOG was also used for this parent using the same parameters as used in MELTS. The effect of adding H_2O to the initial melt was also tested using PETROLOG.

Location 4. 10° N – 10.6° N

The final sub-region consists of 479 glass analyses. The parent sample chosen was WASRAI2-066-001 *Niu et al.,* (1997). All PETROLOG parameters remained the same as for location 1.

RESULTS

Effects of Varying MgO Content in Parental Magma, Location 1

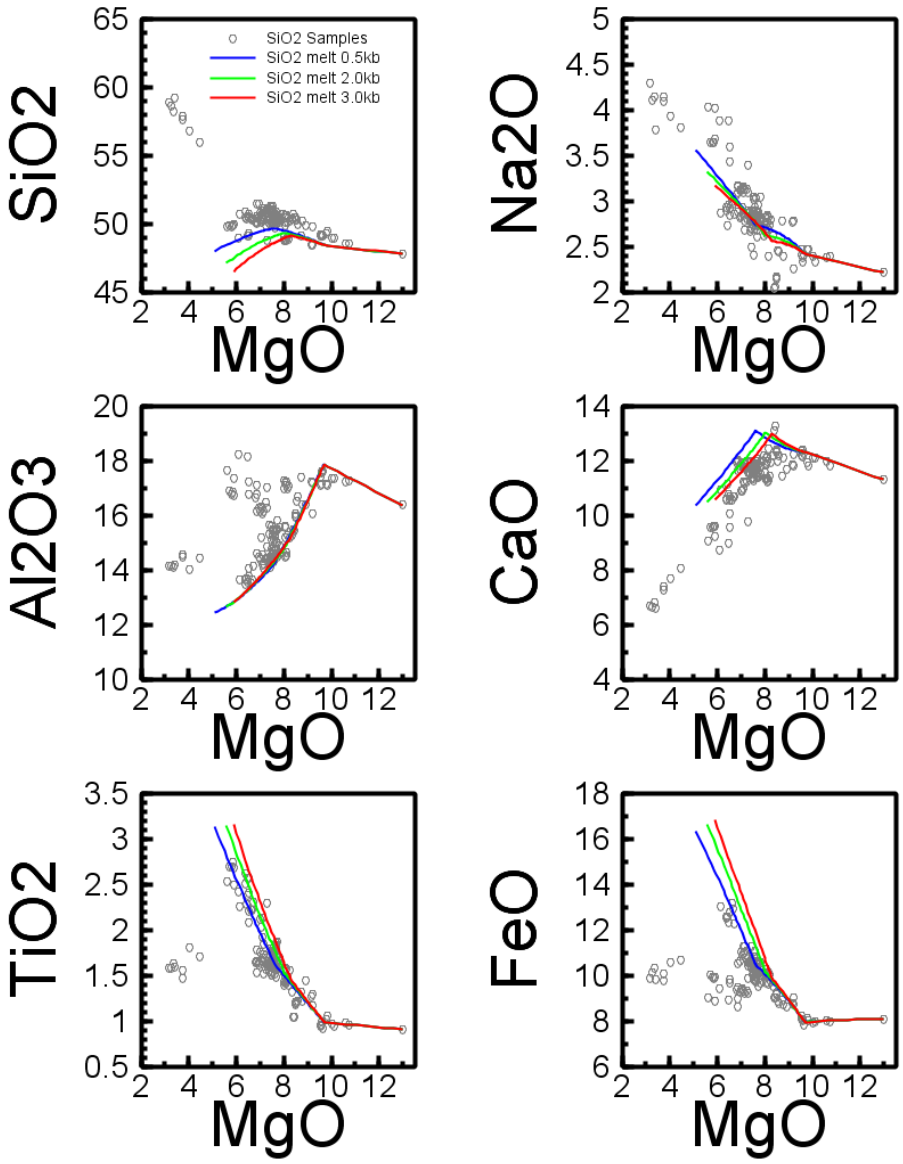

Figure 3. Weight % of major oxides for glasses sampled from 8.3°N to 8.8°N along the EPR compared with liquid compositions calculated using PETROLOG *Danyushevsky and Plechov,* (2011) using high MgO parent ALV2384-001 *Perfit et al.,* (1996) at various pressures. Blue lines represent crystallization occurring at 0.5kb, green at 2.0kb, and red at 3.0kb.

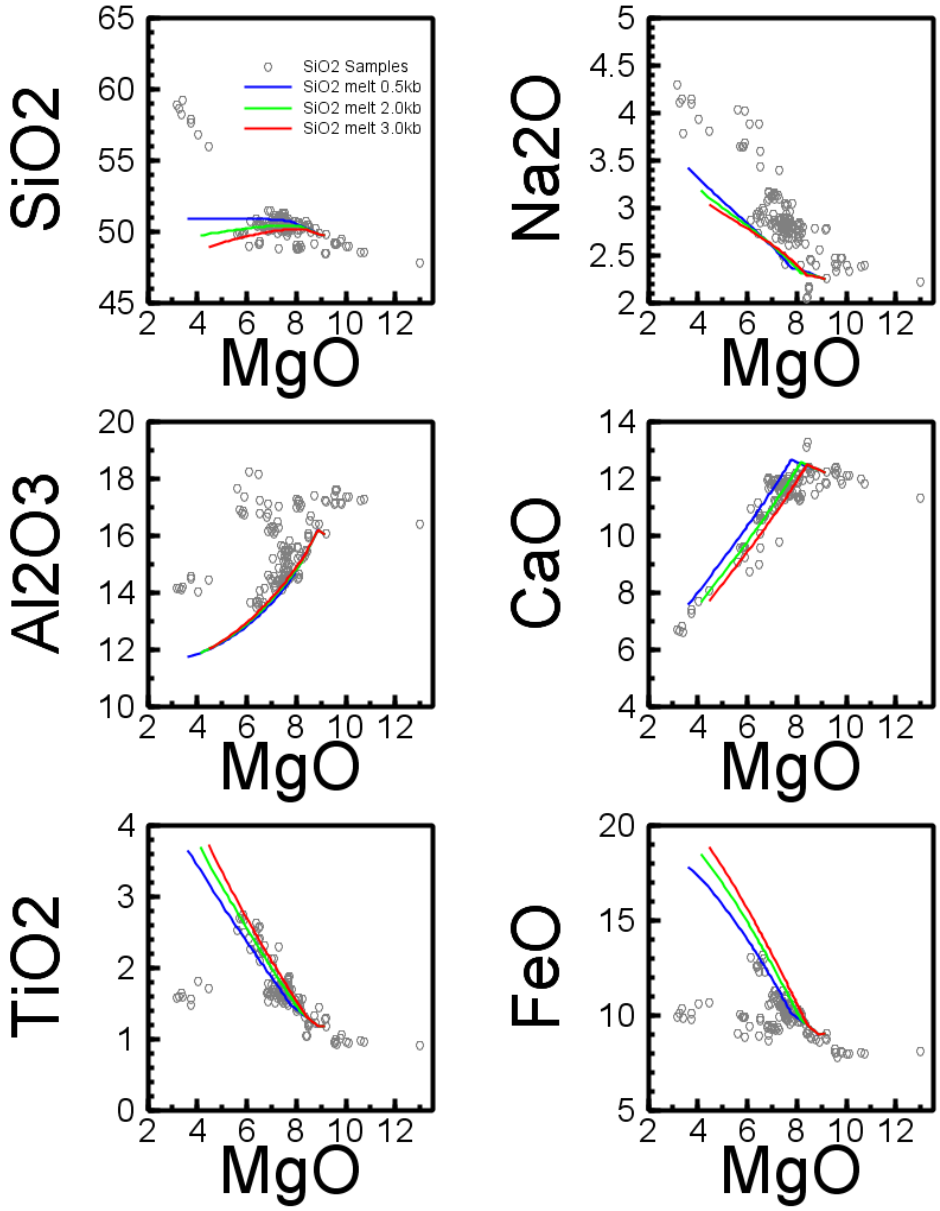

Figure 4. Weight % of major oxides for glasses sampled from 8.3°N to 8.8°N along the EPR compared with liquid compositions calculated using PETROLOG *Danyushevsky and Plechov,* (2011) using low MgO parent WASSIQR-003 *Natland et al.,* (1989)at various pressures. Blue lines represent crystallization occurring at 0.5kb, green at 2.0kb, and red at 3.0kb.

Effects of Fe-Ti Oxides and Oxygen Fugacity, Location 2

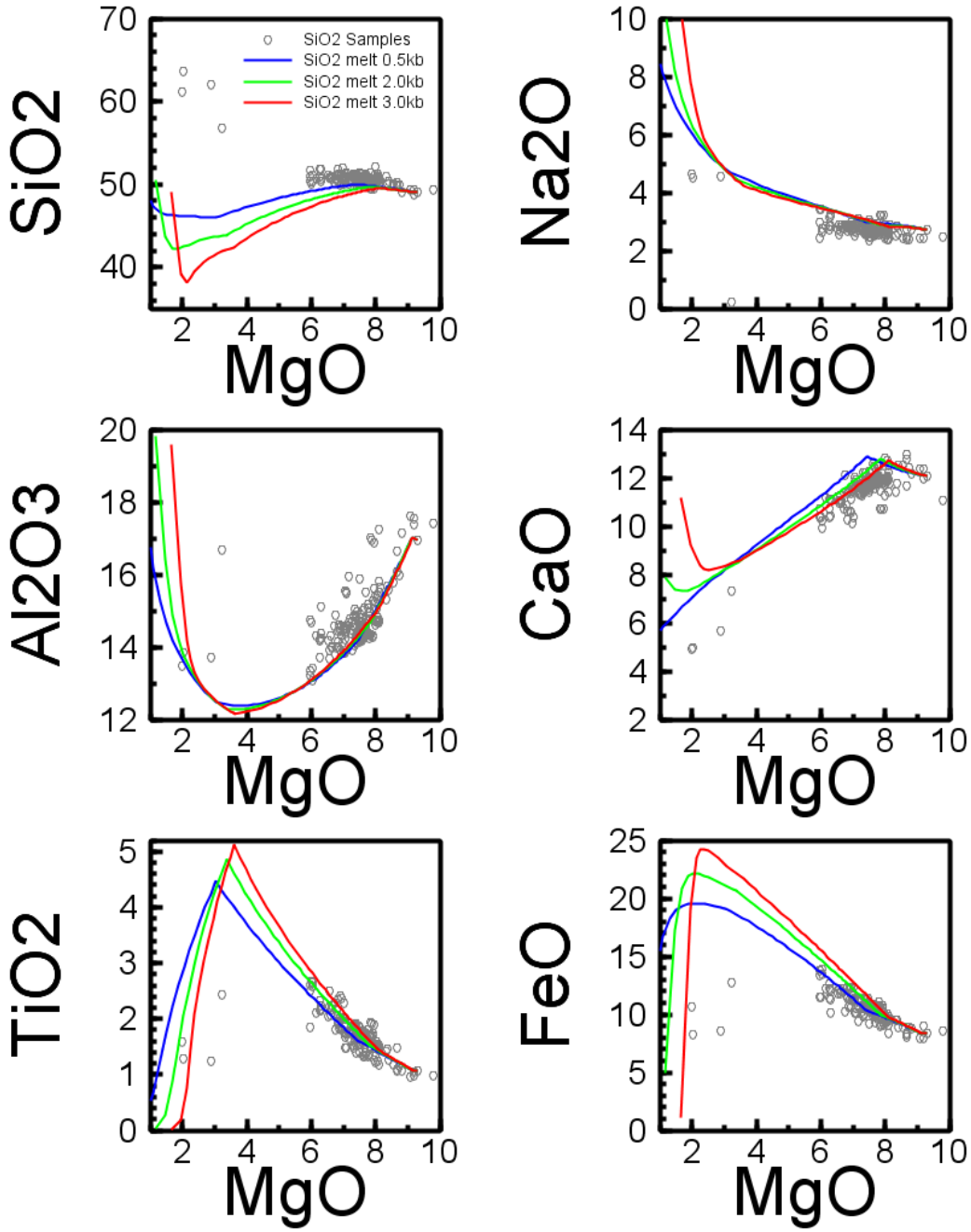

Figure 5. Weight % of major oxides for glasses sampled from 8.8°N to 9.4°N along the EPR compared with liquid compositions calculated using PETROLOG *Danyushevsky and Plechov*, (2011) and crystallizing Fe-Ti oxides at a QFM buffer of -1. Blue lines represent crystallization occurring at 0.5kb, green at 2.0kb, and red at 3.0kb.

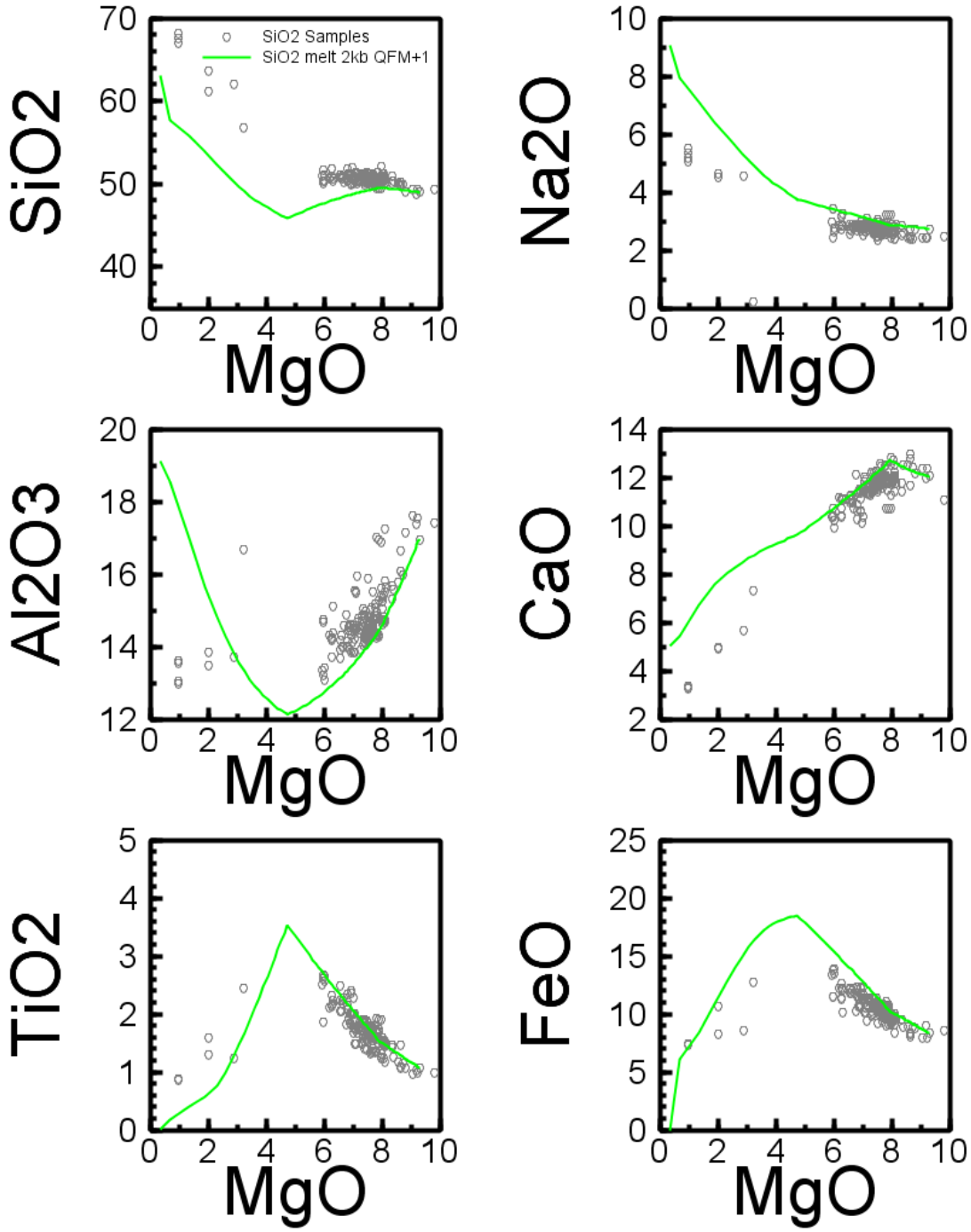

Figure 6. Weight % of major oxides for glasses sampled from 8.8°N to 9.4°N along the EPR compared with liquid compositions calculated using PETROLOG *Danyushevsky and Plechov*, (2011) and crystallizing Fe-Ti oxides at a QFM buffer of +1. Crystallization was calculated at 2kb.

Effects of Varying H_2O Content of Initial Melt, Location 3

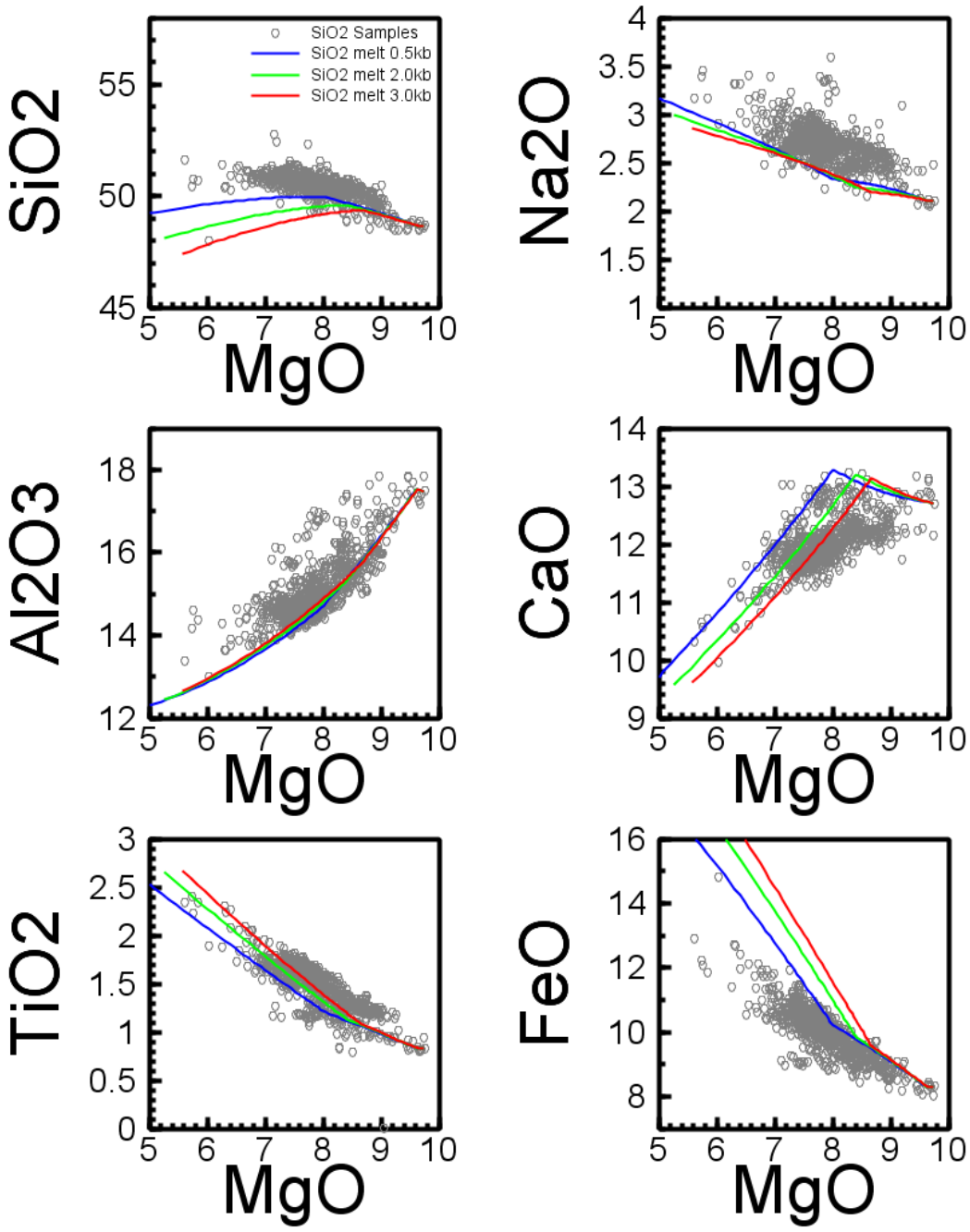

Figure 7. Weight % of major oxides for glasses sampled from 9.4°N to 10°N along the EPR compared with liquid compositions calculated using PETROLOG *Danyushevsky and Plechov*, (2011) at various pressures for parent AII0112-25-003-002 *Allan et al.*, (1989) . Blue lines represent crystallization occurring at 0.5kb, green at 2.0kb, and red at 3.0kb.

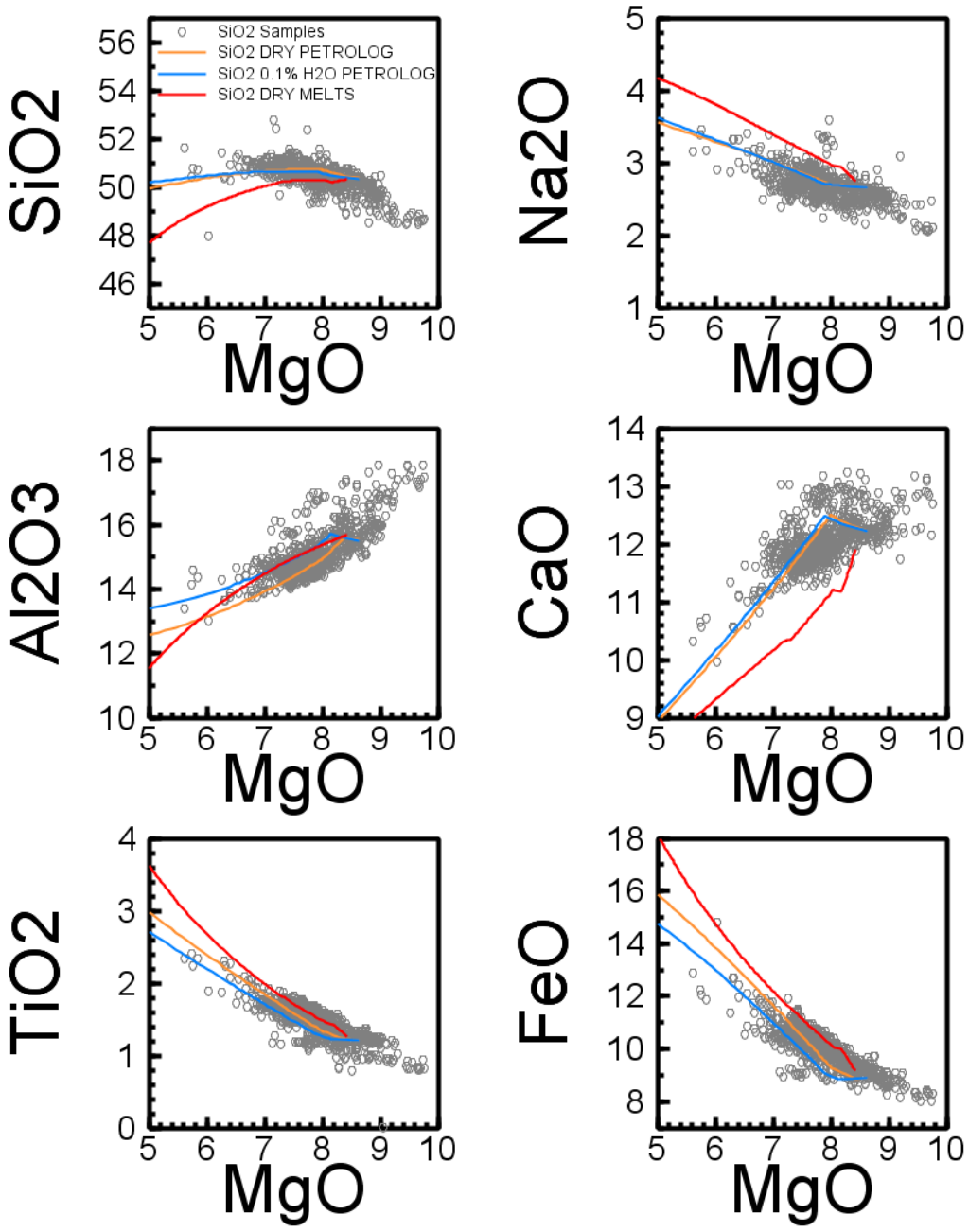

Figure 8. Weight % of major oxides for glasses sampled from 9.4°N to 10°N along the EPR compared with liquid compositions calculated using PETROLOG *Danyushevsky and Plechov*, (2011) and MELTS *Ghiorso and Sack*, (1995), and comparing the effect of adding H_2O to the initial melt AII131-11-R455GL *Perfit*, (2000). Orange lines represent PETROLOG calculations done with no added H_2O. Blue lines represent PETROLOG calculations done with 0.1% H_2O added to the initial melt. Red lines represent calculations done using MELTS with no added H_2O. All calculations were done at 2.0kb.

Location 4 10° N – 10.6° N

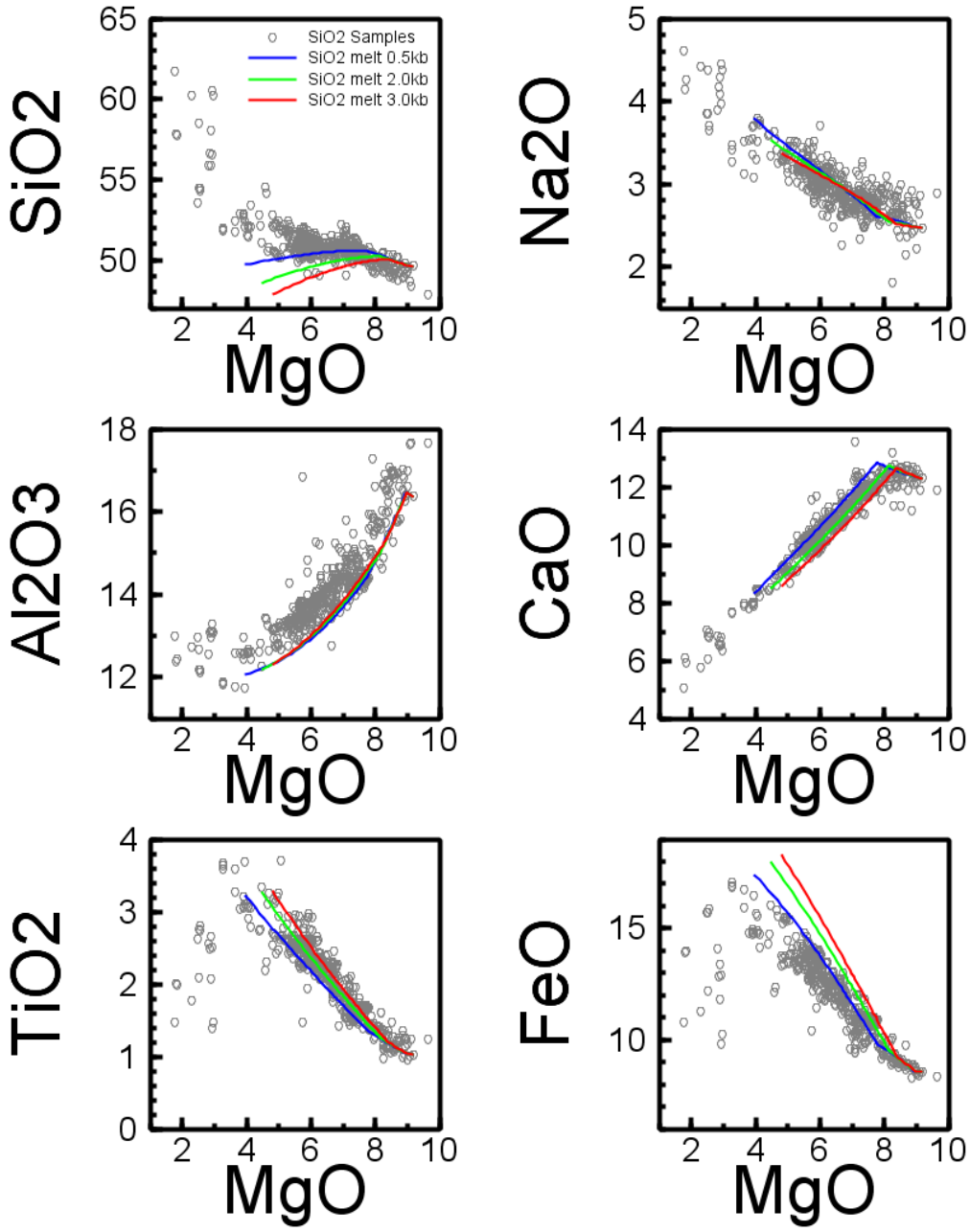

Figure 9. Weight % of major oxides for glasses sampled from 10°N to 10.6°N along the EPR compared with liquid compositions calculated using PETROLOG *Danyushevsky and Plechov,* (2011) at various pressures. Blue lines represent crystallization occurring at 0.5kb, green at 2.0kb, and red at 3.0kb.

DISCUSSION

Location 1

The location between 8.3°N and 8.8°N was chosen to compare the differences in the calculated liquid compositions for two different parental magmas. This location was chosen largely due to the existence of one sample; ALV2384-001 *Perfit et al.,* (1996) with nearly 13 wt. % MgO, the least evolved sample from any of the four sub-regions. This presented the perfect opportunity to learn how the model reacts to the choice of a very primitive parent composition. Some of the calculated trends are unaffected by changes in starting MgO, such as FeO, TiO_2, and Al_2O_3 (Fig. 3–4). For the low MgO parent (WASSIQR-003, Figure 4) the calculated Na_2O contents are higher than the values in analyzed glasses and this is probably due to the parent being anomalously low in Na_2O because the slope for the natural samples is very similar to the slope of the calculated lines on the plot of Na_2O versus MgO. If the parent had a higher Na_2O content, the calculated lines would fit very well with the natural samples. The CaO and SiO_2 contents of the calculated liquids, however, do seem to be strongly affected by the composition of the parent. CaO perhaps is not unexpected as the onset of clinopyroxene crystallization determines how closely the calculated line falls to the natural sample data. Calculated lines for the low MgO parent (WASSIQR-003, Figure 4) shows much closer agreement with CaO data for the natural samples than the calculated lines for the high MgO parent *(*ALV2384-001, Figure 3). Predicted SiO_2 contents of liquids produced from the high MgO parent (Figure 3) decrease once MgO< 8 wt. %, and there is poor correlation between calculated and observed SiO_2 contents. Furthermore, as pressure increases the SiO_2 contents of the calculated liquids move further from the compositions of the natural samples. In contrast, the SiO_2 contents of liquids produced from the low MgO parent (Figure 4) agree well with the contents observed in the natural samples. For these reasons, I believe that modeling works better using parents with compositions close to

those of natural samples lying at the high MgO end of the data array. For this location, the observed major oxide compositions of the natural samples (with the exception of Na_2O) is spanned by the three chosen pressures of crystallization (0.5–3 kb). For this reason, I believe a mid-range pressure (1.5–2.0) kb would result in the best fit at this locality.

Location 2

The sub-region between 8.8°N and 9.4° yielded the most consistent fits of calculated liquid compositions to those of natural samples of the four locations studied. Calculated liquid compositions agree reasonably well with data for the natural glasses and suggest crystallization at a pressure of 2 kb. However, the FeO and TiO_2 concentrations in the evolved compositions require that Fe-Ti oxides, ilmenite and magnetite, are part of the crystallizing assemblage (Figures 5 & 6) is. The crystallization of these minerals is also required to explain the low TiO_2 and FeO values for evolved samples at locations 1 & 4. Calculated liquid composition produced by increasing the oxygen fugacity (fO_2) of the initial melt (Figure 6) shows that crystallization of ilmenite and magnetite can even explain the relatively high SiO_2 values of evolved samples from all sub-regions. I suggest that a pressure of 2kb–3kb best explains the compositions of the majority of the natural samples at this locality.

Location 3

The section of ridge between 9.4°N and 10°N is one of the most heavily sampled and studied in the world and provided by far the largest in sample size in this study. PETROLOG modeling of fractional crystallization in this region across a range of pressures has been reported in previous work *Goss et al.*, (2010). The results of *Goss et al.* and that performed herein yield very similar results. The calculated liquids in this study using a high-MgO parent indicate crystallization at 2 kb for most oxides, however, these liquids contain higher FeO than the majority of samples from

the region, even at the lowest pressure of 0.5 kb used in the modeling. In contrast, liquids calculated by *Goss et al*. (2010) show that the calculated FeO contents are comparable to those of the natural glass samples at pressures ranging from 0.5 to 4 kb. A possible explanation of this is that the fO_2 values in the *Goss et al.* (2010) calculations were equal to QFM=0, whereas in the calculations performed herein the fO_2 was set at QFM=-1.

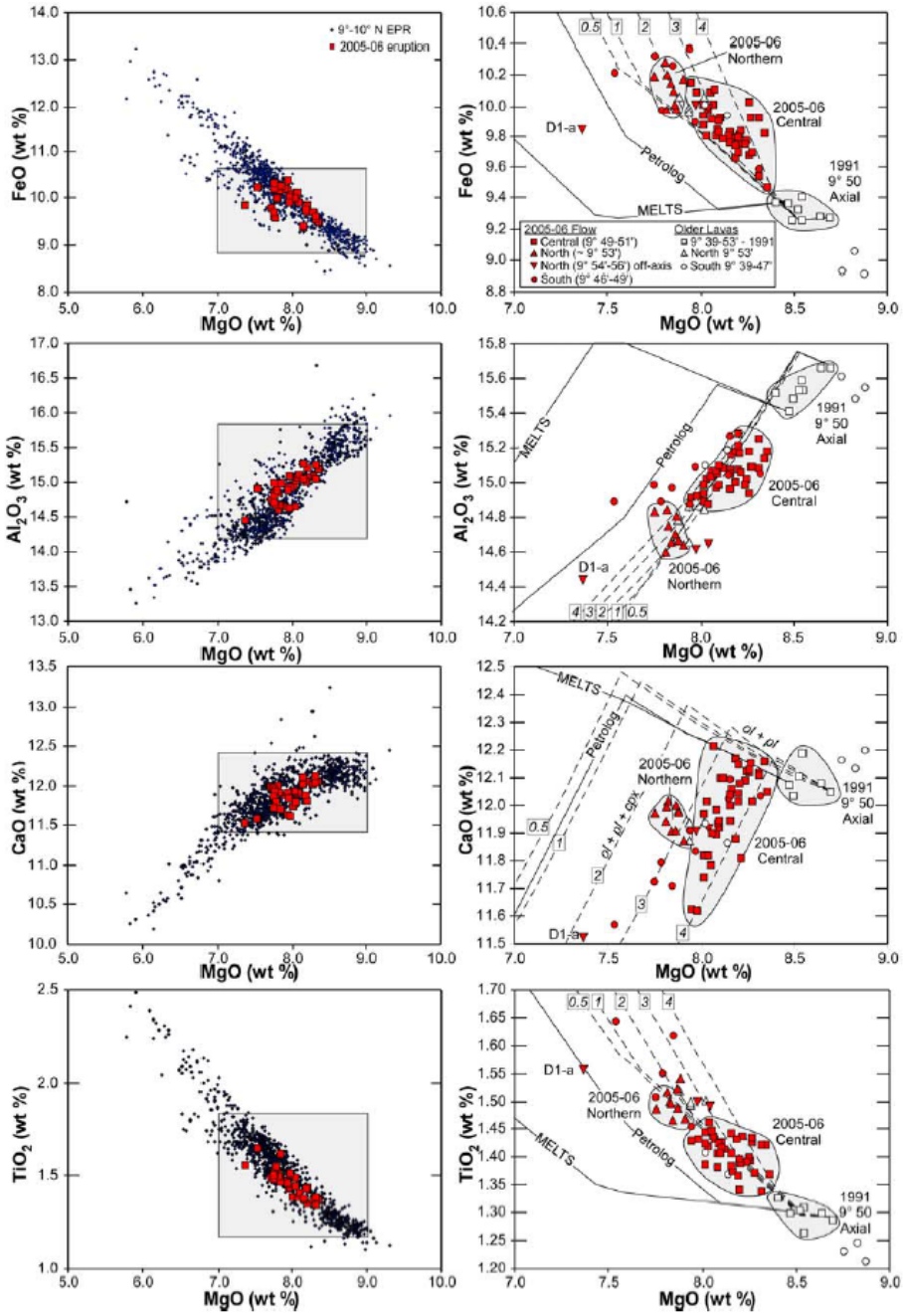

Figure 10. Plots of Al_2O_3, CaO, FeO, and TiO_2 between 9°N and 10°N along the East Pacific Rise. Dashed lines show PETROLOG and MELTS calculated liquid compositions at various pressures of crystallization. Figure from *Goss et al.* (2010).

Calculations at 2 kb using a different parent, AII131-11-R455GL *Perfit*, (2000), with lower MgO, yield liquid compositions that agree well with the compositions of glass samples. Crystallization was also modeled for this parent using the MELTS software package of *Ghiorso*

and Sack, (1995) for comparison the work of *Goss et al.* (2010), who also modeled crystallization along this segment using both PETROLOG and MELTS. The fit between the liquid compositions calculated with MELTS and the glass data is not as good as that obtained using PETROLOG, supporting the results reported by *Goss et al*. (2010) (Figure 10). MELTS suppresses the crystallization of olivine at high MgO, which drove the calculated CaO values down, and Na_2O values up much too quickly to agree with the natural samples (Figure 8). Modeling was also done at 2kb using PETROLOG to explore the effects of adding small amounts of H_2O to the initial melt. Adding 0.1 wt. % H_2O to the melt only had a significant effect on Al_2O_3. Addition of H_2O to magmas suppresses the crystallization of plagioclase, and to a lesser extent, clinopyroxene (Figure 8). This is a likely explanation for why the Al_2O_3 contents of calculated liquids for all four segments are slightly lower than the values for natural samples. Even small but reasonable values of 0.025–0.075 wt. % H_2O in the initial melt would likely improve the "fits" for Al_2O_3 for all segments, without being detrimental to the fits for other major oxides.

Location 4

At the last location modeling was only done for a system crystallizing olivine, plagioclase, and clinopyroxene at 0.5kb, 2kb, and 3kb (Figure 9). The "fit" for Na_2O is very good at this location, reinforcing the suggestion that the poor "fit" for Na_2O at location 1 is the result of anomalously low Na_2O in the parent composition and not due to other assumptions inherent in the modeling. The end result is similar to location 1 (Figure 4), and suggests that low pressure crystallization (0.5kb–2.0kb) best explains the observed range of compositions in the natural glass samples.

CONCLUSIONS

The Siqueiros and Clipperton transforms are the major topographic features of the East Pacific Rise at latitudes from 8.3°N to 10.6°N. The role that transforms play in the evolution of basalts formed at mid-ocean ridges could not be determined by the modeling done in this study alone. The goal of this study was to determine whether crystallization of olivine, plagioclase, and clinopyroxene from a single parental composition could produce a range of major oxide compositions that is consistent with the compositions of analyzed glasses. Successful models allow provide estimates of the pressure of partial crystallization, and hence the depth of partial crystallization. The results presented in this thesis indicate that crystallization of olivine, plagioclase, and clinopyroxene from basalts, with ilmenite and magnetite in basaltic andesites and dacites, at low to moderate pressures (0.5kb–2.0 kb) can explain the compositions of the majority of samples along this section of the EPR. Small variations in H_2O content and oxygen fugacity of the parent magmas improves agreement between calculated liquid compositions and analyzed glass compositions. There is also the possibility that mixing of magmas and assimilation of crustal material have occurred in addition to fractional crystallization. This is suggested by comparison of the predicted K_2O and P_2O_5 contents of liquids produced in crystallization models with the actual K_2O and P_2O_5 contents of glasses (See Figures in Appendices A–D) . The poor agreement between calculated and actual K_2O and P_2O_5 contents for at least some segments could indicate that the concentrations of these highly incompatible oxides reflects processes other than crystallization. *Zerda* (2016) and *Sethna* (2016) concluded that assimilation and mixing had affected the compositions of basalts erupted along the nEPR.

RECOMMENDATIONS FOR FUTURE WORK

The first step to a more complete understanding of the nEPR would be to continue to fine-tune the parameters of the PETROLOG model. There probably exists some combination of pressure, H_2O content, and fO_2 that will yield a best fit for each segment of the ridge. A shortcoming of modeling in general is the inability to characterize the effects of mixing and assimilation. All of the sub-regions in this study contained samples which cannot be explained by the process of crystallization alone, and other work done recently on this region of the EPR support the conclusion that crystallization was accompanied by mixing and assimilation *Zerda* (2016); *Sethna* (2016). To identify the operation of processes other than crystallization, a detailed study of the geochemistry of the magmas erupted in this area is required. Detailed studies of both stable and radiogenic isotopes along with trace elements is needed to examine and quantify the roles of the different processes involved in magma evolution.

REFERENCES CITED

Allan, J. F., Batiza, R., Perfit, M.R., Fornari, D.J., and Sack, R.O. (1989) Petrology of Lavas from the Lamont Seamount Chain and Adjacent East Pacific Rise, 10° N. J Petrology, 30 (5): 1245-1298. doi: 10.1093/petrology/30.5.1245.

Ariskin, A.A., and Barmina, G.S. (1999) An empirical model for the calculation of spinel-melt equilibria in mafic igneous systems at atmospheric pressure: 2. Fe-Ti oxides, Contrib. Mineral. Petrol., 134, 251–263, doi:10.1007/s004100050482.

Asimow, P.D., and Ghiorso, M.S. (1998) Algorithmic modifications extending MELTS to calculate subsolidus phase relation. American Mineralogist, 83, 1127-1131.

Bowen, N.L. (1956). The Evolution of the Igneous Rocks. Canada: Dover. 332 pp.

Danyushevsky, L. V. (2001) The effect of small amounts of H_2O on crystallisation of mid-ocean ridge and back-arc basin magmas, J. Volcanol. Geotherm. Res., 110, 265–280, doi:10.1016/S0377-0273(01)00213-X.

Danyushevsky, L.V., and Plechov P. (2011) Petrolog3: Integrated software for modeling crystallization processes, Geochem. Geophys. Geosyst. 12. Q07021, doi:10.1029/2011GC003516.

Ghiorso, M.S., and Sack, R.O. (1995) Chemical mass transfer in magmatic process. IV. A revised and interally consistent thermodynamic model for the interpolation and extrapolation of liquid-solid equilibria in magmatic systems at elevated temperatures and pressures. Contributions to Mineralogy and Petrology, 119,197-212.

Giordano, D., and Dingwell, D. B. (2003) The kinetic fragility of natural silicate melts. Journal of Physics: Condensed Matter, 15, S945

Goss, A. R., Perfit, M.R., Kamenov, G.D., Fundis, A., Ridley, W.I., Rubin, K.H., Soule, S.A., and Fornari, D.J. (2010) Geochemistry of lavas from the 2005-2006 eruption at the East Pacific Rise, 9°46'N-9°56'N: Implications for ridge crest plumbing and decadal changes in magma chamber compositions, Geochem. Geophys. Geosys., 11(5), 35. doi: 10.1029/2009GC002977

Herzberg, C. (2004) Partial Crystallization of Mid-Ocean Ridge Basalts in the Crust and Mantle, J. Petrol., 45(12), 2389-2405.

Kress, V.C., and Carmichael, I.S.E. (1988) Stoichiometry of the iron oxidation reaction in silicate melts. American Mineralogist, 73, 1267-1274.

Lange, R.A. and Carmichael, I.S.E. (1987) Densities of Na_2O-K_2O-CaO-MgO-FeO-Fe_2O_3-Al_2O_3-TiO_2-SiO_2 liquids: new measurements and derived partial molar properties. Geochimica et Cosmochimica Acta, 51, 2931-2946.

Macdonald, K.C. (2001) Seafloor Spreading: Mid-Ocean Ridge Tectonics, in in Encyclopedia of Ocean Sciences, 100-117, Academic Press.

Natland, J.H. (1989) Partial melting of a lithologically heterogeneous mantle, 1: Inferences from crystallization histories of magnesian abyssal tholeiites from the Siqueiros Fracture Zone. In: Saunders, A.D. and Norry, M. (eds), Magmatism in the Ocean Basins: Geol. Soc. London, Spec. Publ. 42: 41-77.

Niu, Y., Langmuir, C.H., and Kinzler, R.J. (1997) The origin of abyssal peridotites: a new perspective. Earth and Planetary Science Letters, 152, 251-265.

Perfit M. R., Fornari, D.J., Ridley, W.I., Kirk, P.A., Casey D.J., Kastens, K.A., Edwards, M., Shuster, R., and Paradis, S., (1996). Recent volcanism in the western Siqueiros Transform Fault: Picritic basalts and implications for MORB magma genesis. Earth Planet Sci. Lett., 141, 91-108.

Perfit, M. R., (2000) Major element compositions of basalt glasses from the east pacific rise, 9° N, unpublished data http://www.earthchem.org/petdbweb/search/ref_info.jsp?Singlenum=816.

Sethna, L. (2016), Geochemistry of Magmas Erupted along the Northern East Pacific Rise at 6°-12°. Implications for Mantle Source Regions and Intracrustal Evolutionary Processes, 50 pp, The Ohio State University, Columbus, Ohio.

Yoder, H. S. and Tilley, C. E. (1962). Origin of basalt magmas: an experimental study of natural and synthetic rock systems. *J. Petrol.*, 3, 342–532.

Zerda, C. (2016), An Integrated Petrological and Geochemical Approach to Understanding Magmatism Along the East Pacific Rise, 75pp, The Ohio State University, Columbus, Ohio.

APPENDIX A

Location 1 8.3°N-8.8°N

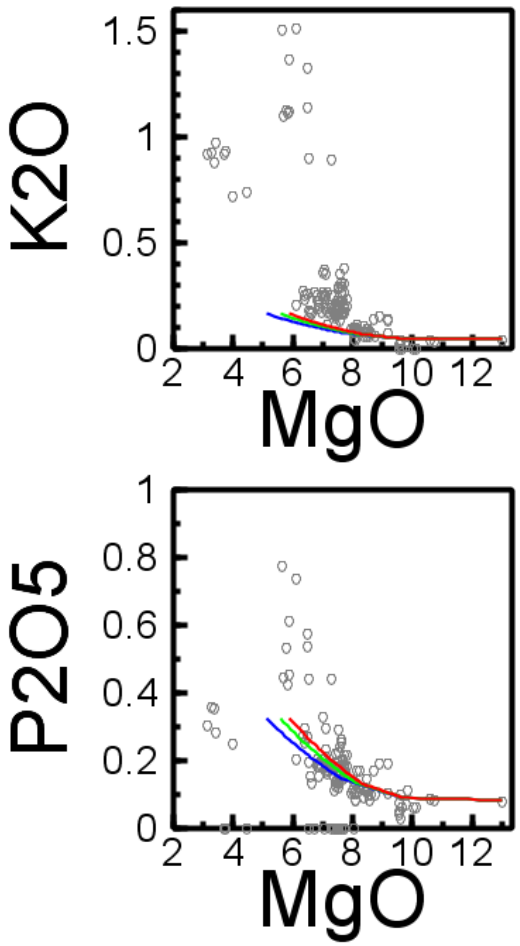

Figure 11. Plots of K_2O and P_2O_5 vs. MgO from glasses sampled from 8.3°N to 8.8°N along the EPR crystallizing at various pressures for a parent magma with relatively high MgO. Blue lines represent 0.5kb, green lines represent 2.0kb, and red lines represent 3.0kb.

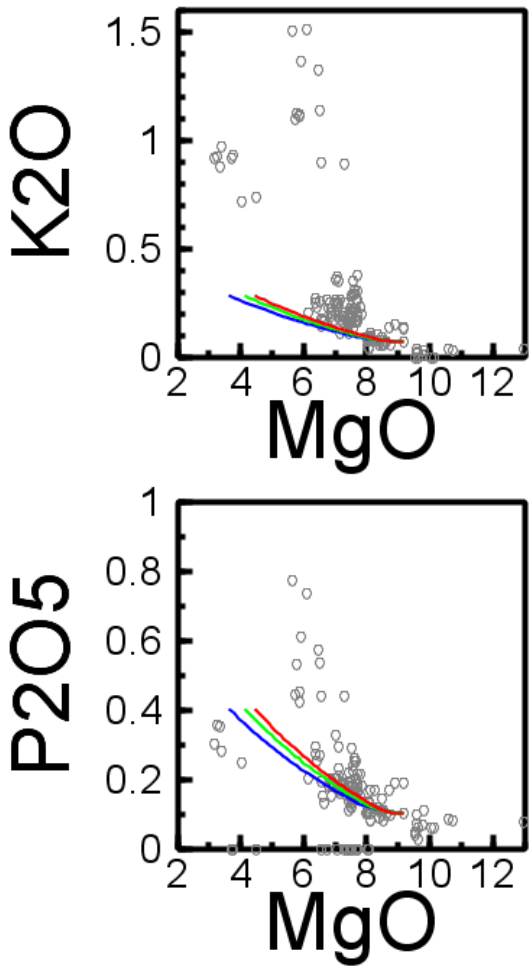

Figure 12. Plots of K_2O and P_2O_5 vs. MgO from glasses sampled from 8.3°N to 8.8°N along the EPR crystallizing at various pressures for a parent magma with relatively lower MgO. Blue lines represent 0.5kb, green lines represent 2.0kb, and red lines represent 3.0kb.

APPENDIX B

Location 2 8.8°N-9.4°N

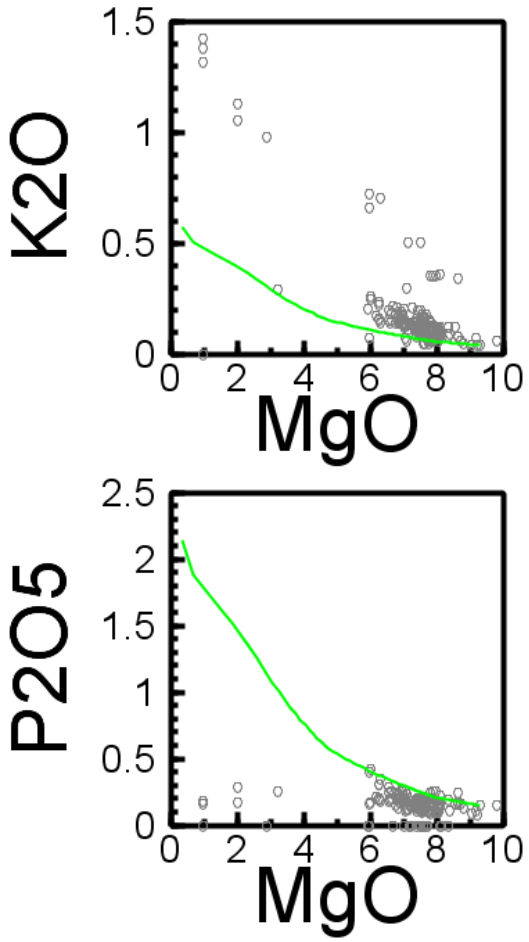

Figure B1. Plots of K_2O and P_2O_5 vs. MgO from glasses sampled from 8.8°N to 9.4°N along the EPR crystallizing Fe-Ti oxides at various pressures with a fO_2 value equal to -1. Blue lines represent 0.5kb, green lines represent 2.0kb, and red lines represent 3.0kb.

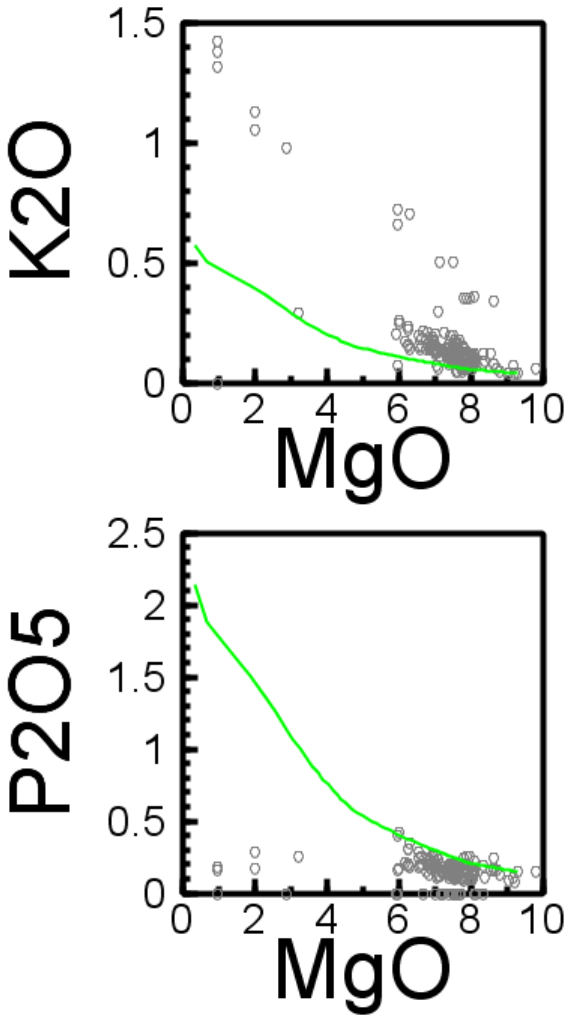

Figure B2. Plots of K_2O and P_2O_5 vs. MgO from glasses sampled from 8.8°N to 9.4°N along the EPR crystallizing Fe-Ti oxides with a fO_2 value equal to +1. Green lines represent crystallization at 2.0kb.

APPENDIX C

Location 3 9.4°N-10°N

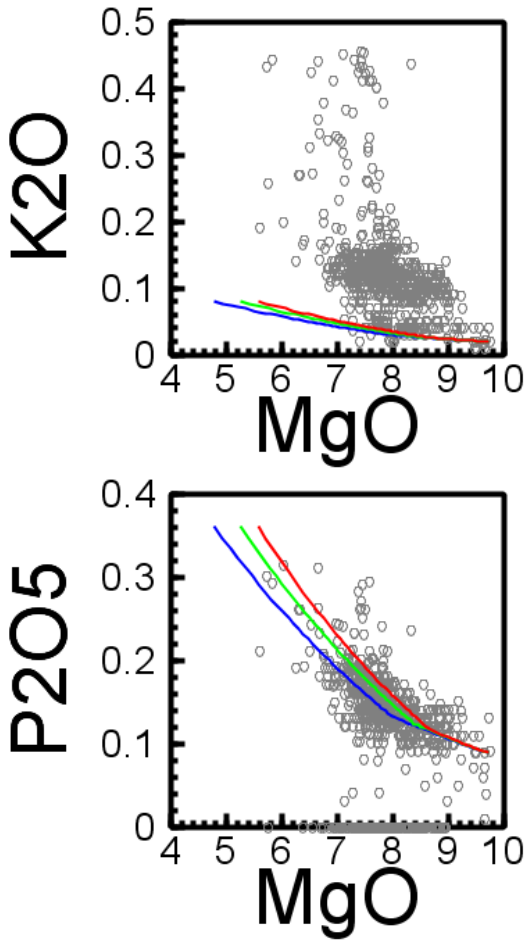

Figure C1. Plots of K_2O and P_2O_5 vs. MgO from glasses sampled from 9.4°N to 10°N along the EPR. Blue lines represent 0.5kb, green lines represent 2.0kb, and red lines represent 3.0kb

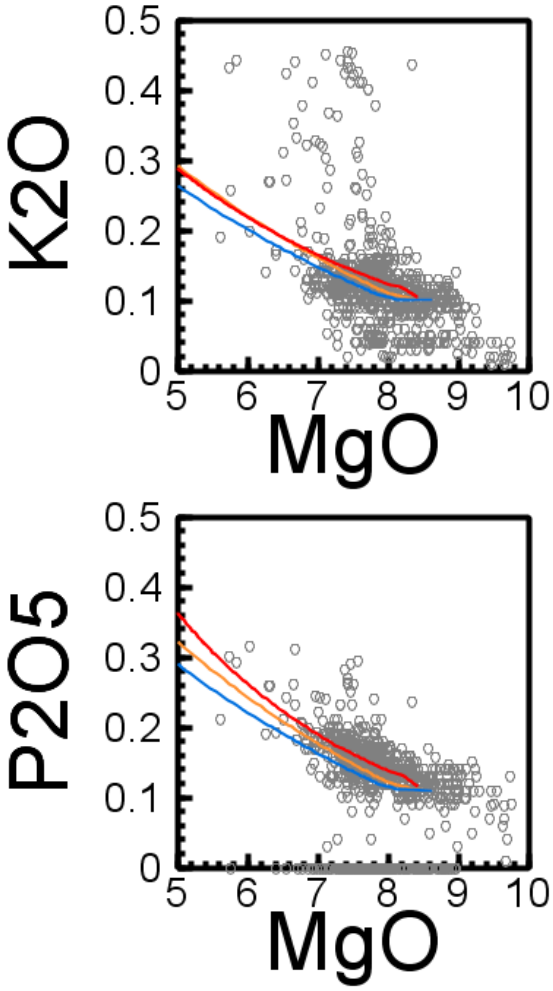

Figure C2. Plots of K_2O and P_2O_5 vs. MgO from glasses sampled from 9.4°N to 10°N along the EPR. Orange lines represent PETROLOG calculations done with no added H_2O. Blue lines represent PETROLOG calculations done with 0.1% H_2O added to the initial melt. Red lines represent calculations done using MELTS with no added H_2O. All calculations were done at 2.0kb.

APPENDIX D

Location 4 10°N-10.6°N

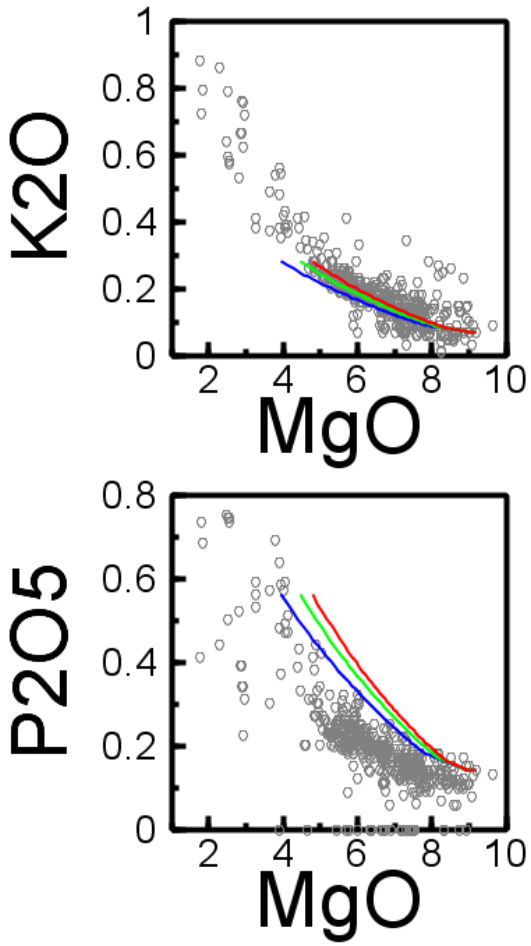

Figure D1. Plots of K_2O and P_2O_5 vs. MgO from glasses sampled from 10°N to 10.6°N along the EPR. Blue lines represent crystallization occurring at 0.5kb, green at 2.0kb, and red at 3.0kb